JOURNAL OF MATERIALS SCIENCE **40** (2005) 4333–4339

Fabrication of ferrous metallic foams by reduction of ceramic foam precursors

A. VERDOOREN, H. M. CHAN*, J. L. GRENESTEDT, M. P. HARMER, H. S. CARAM
Center for Advanced Materials and Nanotechnology, Lehigh University, Bethlehem PA, USA
E-mail: helen.chan@lehigh.edu

A process has been developed for obtaining closed cell metallic foams using a ceramic foam precursor. In the present study, the major constituent of the ceramic foam precursor was iron oxide (Fe_2O_3), which was mixed with various foaming/setting additives. The mixture set rapidly at room temperature, stabilizing the foam generated by hydrogen release. The oxide foam was then reduced by annealing at 1240°C in a non-flammable hydrogen/inert gas mixture to obtain a metallic foam with a relative density of 0.23 ± 0.017, and an average cell diameter of 1.32 ± 0.32 mm. The iron foams were tested in compression and yielded an average compressive strength of 29 ± 7 MPa. The compressive stress-strain curves obtained were typical of cellular metals. The normalized strengths of the metal foams obtained in the present study compare favorably with those of steel foams produced by other techniques.

1. Introduction

Metal foams possess special characteristics which render them attractive for a large range of applications; these include lightweight structures, energy absorption, and thermal management [1]. The properties and uses of foams and cellular materials have been the subject of several extensive reviews [1–5]. With regard to multi-property indices, which are often used in design criteria, metal foams offer a potential for high stiffness and strength, at low density. At any given density, closed cell foams are projected to be stronger and stiffer that open cell structures [4]; accordingly, closed cell foams are preferable for structural applications.

To date, a variety of methods have been used to produce metal foams [1]. Closed cell structures have been obtained by foaming of the molten metal [6] and powder metallurgy (P/M) [7]. In this latter process, compacted metal powders are sintered together, sometimes with the incorporation of blowing agents or trapped gas. Another technique which can be used to generate cellular metallic structures is the consolidation of hollow spheres [8–10]. The hollow metallic spheres may be formed by coating polymeric spheres, or by blowing of metal or metal hydride powder slurries. The production of steel foams presents a particular challenge, since foaming normally can only be achieved at temperatures close to the melting point, which makes the control of the metal foam morphology very difficult. The present work circumvents this problem by developing a new approach to produce a ferrous metallic foam.

Results of preliminary studies on the production of metallic foams from ceramic foam precursors (CFPs) have been reported previously [11]. In this novel method, an iron foam is produced in two stages. The first step, involves the foaming of a mixture made of iron (III) oxide and appropriate additives. The second step is the complete reduction of the ceramic precursor to obtain a metal foam. The CFP process has several potential advantages over existing foam fabrication methods. First of all, foaming is achieved at room temperature which is experimentally convenient. The CFP is produced from low cost raw materials, and the reduction process requires only standard equipment which is already widely used in industry. Furthermore, this process is amenable to scale-up, and complex shapes can be achieved using inexpensive mold materials. The CFP technique is particularly advantageous for high melting point metals, e.g., ferrous alloys, where foaming in the molten state is less attractive from an economic standpoint. It is believed that the foam precursor process is readily adaptable to a wide range of steel compositions. Initial studies, however, were focused on the fabrication of iron-based foams to demonstrate viability.

2. Background

2.1. Production of ceramic foam precursor

The production of the ceramic foam precursor (CFP) is based on a procedure developed by Motoki [12] for preparing a ceramic foam body. This approach involves the reaction of an acidic solution with a metal blowing agent to generate hydrogen; at the same time, cementitious materials react to form a fast setting hydrate. The mixture thus foams and sets simultaneously, enclosing

*Author to whom all correspondence should be addressed.

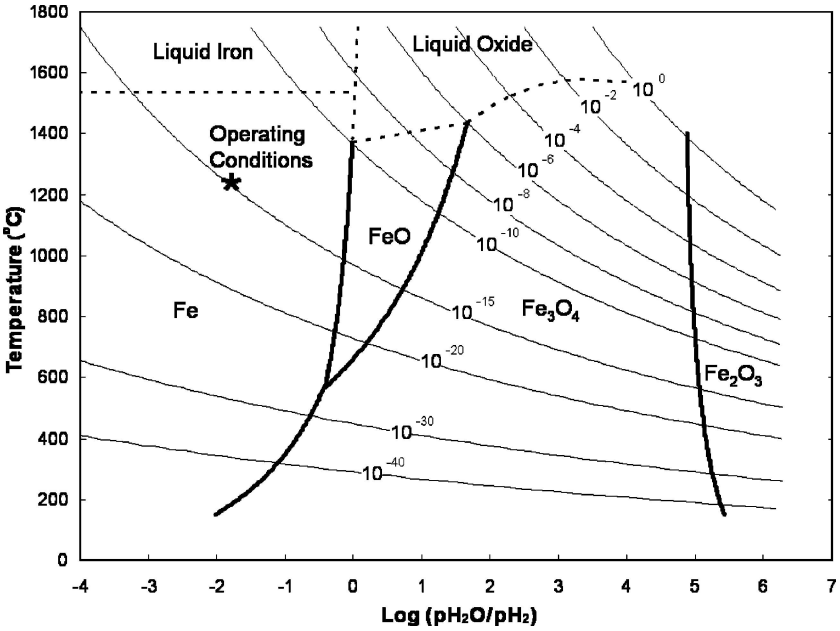

Figure 1 Diagram showing stability fields in the iron/iron oxide system as a function of temperature and ratio of the partial pressure of water and hydrogen (pH_2O/pH_2).

the evolved gas to produce a ceramic foam with a predominantly closed cell structure.

Since the aim of this work was to produce a ferrous foam, a large proportion (> 90 wt%) of iron (III) oxide was added to the list of components initially suggested by Motoki. The other reagents selected for use in this approach were hydrochloric acid, aluminum orthophosphate, calcium oxide, aluminum, and carbon black. The production of the ceramic foam precursor involves two main reactions. The first one relates to the foaming process, in which H_2 is generated as a product of the reaction between Al (blowing agent) and HCl, according to the following stoichiometry:

$$2Al + 6HCl \rightarrow 2AlCl_3 + 3H_2\uparrow \quad (1)$$

The second reaction involves the process to set and harden the precursor. A potential setting mechanism has been proposed based on reactions from analogous systems [13]. This mechanism is based on the following reaction between calcium oxide and aluminum orthophosphate:

$$2CaO + Al(H_2PO_4)_3 \xrightarrow{+H_2O} 2CaHPO_4 \cdot 2H_2O + AlPO_4 \cdot nH_2O \quad (2)$$

The production of $CaHPO_4.2H_2O$ (brushite) causes the setting and hardening of the ceramic precursor. The role of the carbon black is as a foaming stabilizer. Carbon black increases the viscosity of the mixture, which in turn hinders the drainage of the foam and reduces cell coalescence. This ensures that a predominantly closed cell structure is developed.

2.2. Reduction of the ceramic foam

Several authors have studied the reduction of iron (III) oxide (Fe_2O_3) with hydrogen [14–17]. The system under study can be described by the following series of reactions [18]:

$$3Fe_2O_3 + H_2(g) \rightleftarrows 2Fe_3O_4 + H_2O(g) \quad (3a)$$

$$Fe_3O_4 + H_2(g) \rightleftarrows 3FeO + H_2O(g) \quad (3b)$$

$$FeO + H_2(g) \rightleftarrows Fe + H_2O(g) \quad (3c)$$

$$\frac{1}{4}Fe_3O_4 + H_2(g) \rightleftarrows \frac{3}{4}Fe + H_2O(g) \quad (3d)$$

Assuming that the solids are immiscible (unit activity), the nature of the solids present will be completely determined by the ratio of partial pressures of water to hydrogen and can be obtained from the free energies of formation from each of the oxides. For example, for reaction 3(c):

$$FeO \rightleftarrows Fe + \frac{1}{2}O_2(g); \quad K_1 = P_{O_2}^{1/2} \quad (4)$$

$$H_2O(g) \rightleftarrows H_2(g) + \frac{1}{2}O_2(g); \quad K_2 = \frac{p_{O_2}^{1/2} \cdot p_{H_2}}{p_{H_2O}} \quad (5)$$

The expression for K will be given then by K_1/K_2, which reduces to:

$$K = \frac{p_{H_2O}}{p_{H_2}} \quad (6)$$

If the ratio p_{H_2O}/p_{H_2} exceeds the equilibrium constant of the reaction only FeO will be present. Conversely, if this ratio is smaller than K, only Fe will be stable.

Using this procedure, Fig. 1 was generated, which shows the equilibrium conditions between the various components plotted as a function of temperature and p_{H_2O}/p_{H_2}. Note that in terms of establishing the

TABLE I Composition of powder mixture used for the ceramic foam precursor

Component	Weight(%)
Fe_2O_3	95.57
CaO	2.33
Al	1.05
C. Black	1.05

experimental conditions, the value of the oxygen partial pressure is more directly relevant. Accordingly, logarithmic curves representing p_{o_2} isobars were calculated based on Equation 5, and have also been included in the figure. It is readily apparent that the lower the process temperature, the lower the value of p_{o_2} required to reduce the oxide to metallic iron.

3. Experimental procedure

The ceramic foam precursor was produced by mixing 100 ml of an acidic solution (containing HCl, $Al(H_2PO_4)_3$, and H_2O) with 121 g of the following materials in powder form: iron (III) oxide (Fe_2O_3), calcium oxide (CaO), aluminum, and carbon black. The composition of the powder materials is shown in Table I. The acidic solution was a mixture of 12.7 parts of concentrated HCl (hydrochloric acid), 78.8 parts of deionized water, and 8.5 parts of a 50% w/w solution of $Al(H_2PO_4)_3$ (aluminum orthophosphate).

As mentioned previously, foaming occurs by the reaction of aluminum with the acidic solution to generate hydrogen. Due to the presence of setting and bonding materials (CaO and $Al(H_2PO_4)_3$), the mixture foams and sets almost immediately, so that the foam morphology is retained in the green ceramic body. The ceramic foam samples were subsequently dried under ambient temperature conditions for 48 h. Note that results from X-ray powder diffractometry on the dried ceramic foams showed the presence of $CaHPO_4 \cdot 2H_2O$, and hence were consistent with the setting reaction put forward in Equation 2.

Due to safety considerations, it was desirable to utilize a non flammable hydrogen mixture of 4% hydrogen in argon for the reduction process. This gas mixture yields a p_{o_2} in the range of 10^{-15}. Based on Fig. 1, it can be seen that for this value of the oxygen partial pressure, the lowest temperature (in theory) at which complete reduction to Fe could be achieved would be 1000°C. The upper bound temperature is 1567°C, the melting point of iron. Taking into account additional considerations of the reduction kinetics and experimental convenience, a heat-treatment temperature of 1240°C was selected. Cylindrical samples of the ceramic precursor foams, (diameter ∼23 mm, height ∼28 mm), were annealed for 36 h in a tube furnace fitted with end fixtures to achieve atmosphere control. Note that preliminary experiments revealed that complete reduction was achieved for annealing times of 12 h or greater. Results on the effect of annealing time on the degree of reduction and foam microstructure will be reported separately. The volumetric flow rate of the gas mixture was 350 cm^3/min. The heat-up and cool-down rates were 3°C/min.

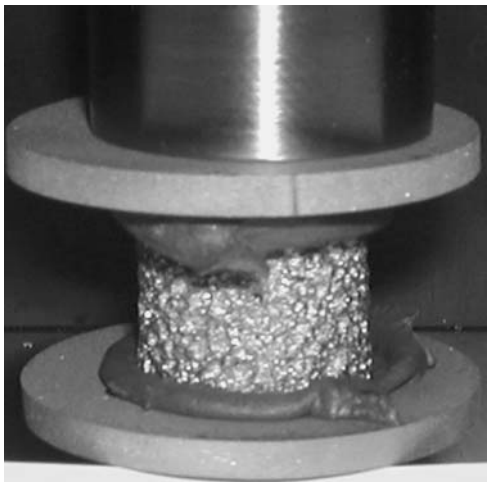

Figure 2 Sample mounted on the ASTM D695 compression subpress.

After reduction, samples of the iron foam were sectioned using a high speed aluminum oxide blade. The specimens were dried and ultrasonically cleaned in ethanol. The sectioned samples were then mounted in a low viscosity epoxy under vacuum conditions. Note that for observation using optical light microscopy, the addition of a black dye to the clear epoxy was found to be beneficial, both in terms of enhanced contrast, and by confining visibility to the sectioned surface. In preparation for metallographic examination, the samples were first ground to 600 grit. They were then sequentially polished with the following: 6 μm diamond, 0.3 μm aluminum oxide, and 0.04 μm colloidal silica. Some specimens were etched in a 2% nital solution (2 parts HNO_3 in 98 parts ethyl alcohol) in order to delineate the grain boundaries in the iron matrix. The cell dimensions of the iron foams were characterized by a combination of image analysis and manual measurement techniques. With the aid of a video camera attachment, optical images of the sectioned and mounted foams were captured using an image analysis program (IA-3001 Image Analysis System fabricated by LECO®). Line segments corresponding to the cell diameters were set manually, but measured by the program. Altogether, more than 360 cells from seven different samples were measured.

Cylindrical samples were tested in an ASTM D695 compression subpress manufactured by Wyoming Test Fixtures. The top and bottom parts of the specimens were glued to a 3.2 mm steel plate to ensure that the test was done on two parallel surfaces (as seen on Fig. 2). The deformation rate used was 1 mm/min. Specimens were compressed until ∼50% strain.

4. Results and discussion

4.1. Foam morphology and microstructure

Using the techniques described above, closed cell, ceramic foam precursors were fabricated. A photograph of the dried CFP is depicted in Fig. 3. Due to the high iron (III) oxide content, the ceramic foams were reddish in color; the cell sizes ranged between 0.5–2 mm. Following the reduction process, the ceramic foams were successfully converted into metallic foams. The corresponding degree of linear shrinkage was 25%.

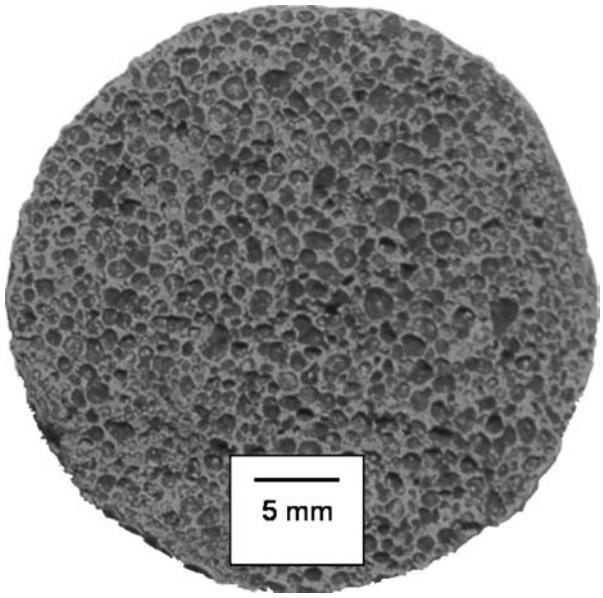

Figure 3 Ceramic foam precursor (CFP).

Samples of the foam were sent out for chemical analysis, and the carbon content of the samples after reduction was determined to be 0.008–0.017%. It is believed that the low carbon content of the reduced samples may be due to the oxidation of solid carbon according to the following reaction:

$$C(s) + O_2(g) \rightleftarrows 2CO(g) \tag{7}$$

The expression for the equilibrium constant will be given by:

$$K_{CO} = \frac{p_{CO}^2}{p_{O_2}} \tag{8}$$

At 1240°C and $p_{O_2} = 10^{-15}$, the equilibrium pressure of CO (p_{CO}) is equal to 11.3 atm. Since the reduction is carried out at ∼1 atm, the reaction as represented by Equation 7 will proceed in the forward direction, producing CO, and therefore diminishing the amount of solid carbon on the sample.

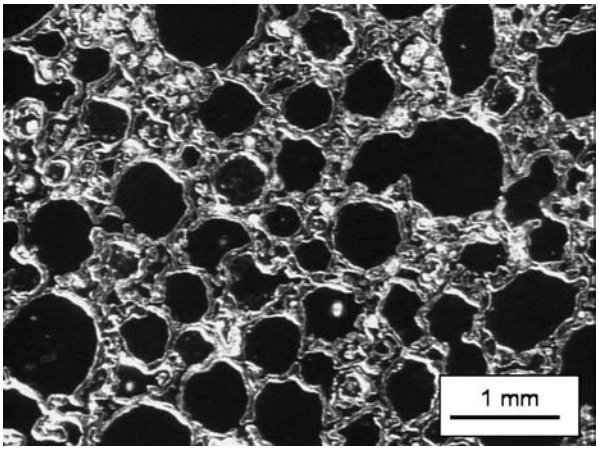

Figure 4 Optical micrograph of polished section of iron foam produced by the reduction of the CFP.

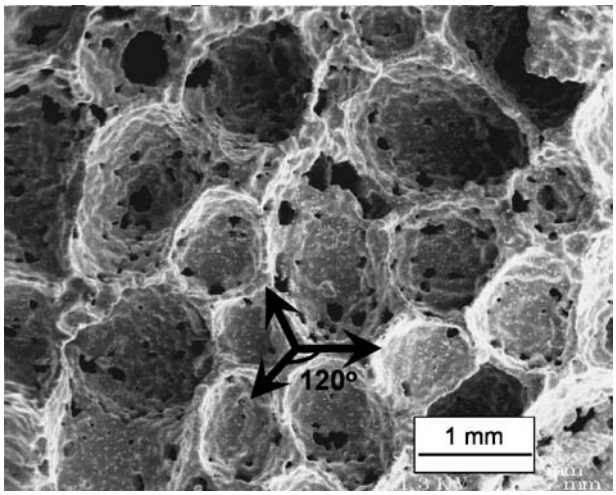

Figure 5 Scanning electron microscope (SEM) micrograph of outer surface of iron foam specimen.

Examination of polished sections confirmed that the morphology was that of a closed cell foam (as seen in Fig. 4). The results of image analysis on the sectioned foams gave an average cell dimension of 1080 ± 260 μm. When corrected for sectioning effects (assuming spherical cells), this corresponds to a cell diameter in the foam of 1320 ± 320 μm [19].

The structure depicted in Fig. 5 shows a scanning electron microscope (SEM) image of the iron foam (taken at 13 kV on a JEOL model JSM-6300F). The weakly polygonal nature of the cells is readily apparent. The iron foam exhibited a predominantly closed wall morphology, although some perforations in the cell walls were also visible. It was observed that in general, the cell walls formed a dihedral angle of ∼120°, which is consistent with the equilibrium rule of foams. Fig. 6 shows a SEM micrograph of the foam taken at higher magnification. It can be seen that the surfaces of the walls were not planar, but rather adopted a 'pin-cushion-like' morphology. Furthermore, a large number of second phase particles can be observed. The inset of Fig. 6 depicts such a particle, shown at

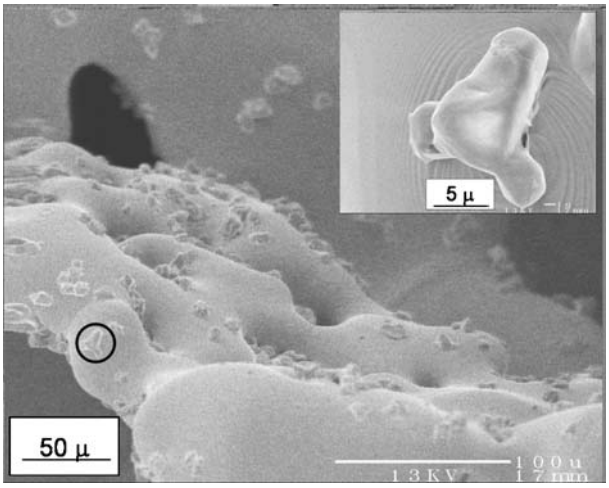

Figure 6 SEM micrograph of a cell wall within the iron foam. Note the presence of second phase particles. Inset shows circled particle at higher magnification.

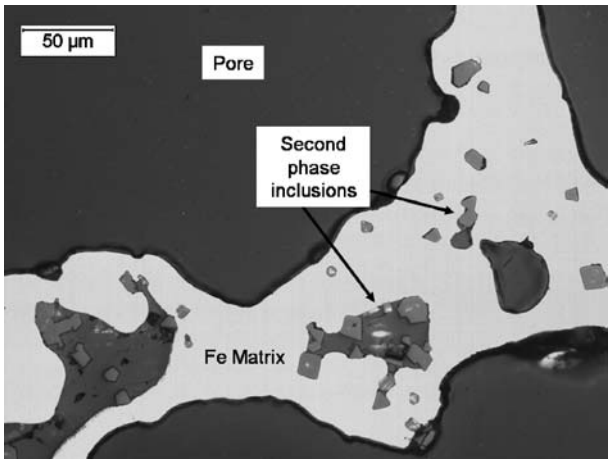

Figure 7 Optical micrograph of a polished section of the iron foam, depicting a cell wall and second phase inclusions.

higher magnification. Optical microscopy of polished sections through the cell walls revealed that the particles were dispersed throughout the ferrite matrix, and not just confined to the surfaces (see Fig. 7). Generally speaking, the inclusions could be categorized as one of two types: they were either highly facetted, with dimensions of the order of 5 to 10 μm, or they were several tens of microns in size, and exhibited a more rounded morphology. Qualitative EDS analysis (Oxford ISIS) of the facetted particles showed the presence of aluminum, oxygen, and iron; it is speculated that they were composed of an iron aluminate spinel ($FeAl_2O_4$). Conversely, the major elements detected by EDS in the particles with the more rounded morphology were calcium, phosphorus, and oxygen. The formation of this kind of Ca-P compound may be due to the thermal decomposition of brushite ($CaHPO_4 \cdot 2H_2O$) which generates calcium pyrophosphate according to the following sequence of reactions [20]:

$$CaHPO_4 \cdot 2H_2O \xrightarrow{100-260^\circ C} CaHPO_4 \xrightarrow{400-440^\circ C} \gamma\text{-}Ca_2P_2O_7 \xrightarrow{1200^\circ C} \beta\text{-}Ca_2P_2O_7 \xrightarrow{1250^\circ C} \alpha\text{-}Ca_2P_2O_7 \quad (9)$$

4.2. Mechanical behavior

A typical stress-strain curve derived from an iron foam sample tested in compression is shown in Fig. 8. The initial (elastic) portion of the curve is linear; this is followed by an extended plateau. The stress level eventually increases due to the densification of the predominantly closed structure of the iron foam. A set of seven iron foam samples was tested, and the compressive strength (σ_c^*) was calculated by taking the load value at an offset of 0.2% strain. The average compressive strength was found to be 29 $\pm$ 7 MPa. This value corresponds to a plateau stress (σ_p^*) equal to 34 $\pm$ 7 MPa. The average density of the samples was equal to 1.83 $\pm$ 0.13 g/cm^3, which corresponds to a relative density of 0.23 $\pm$ 0.017.

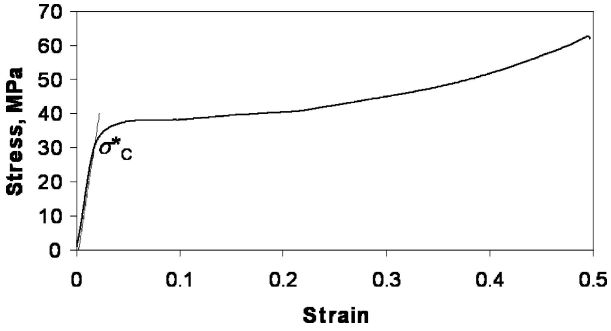

Figure 8 Representative compressive stress-strain curve for metal foam sample.

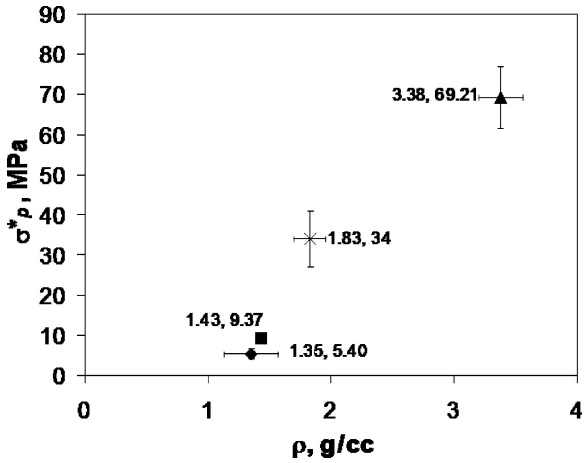

Figure 9 Absolute compressive strength versus absolute density for foams produced by × Present study, ♦ Hollow Spheres [8], ■ Hollow Spheres [9], ▲ P/M [7]. The error bars represent the range corresponding to plus or minus one standard deviation, where no bars are shown the standard deviation lies within the marker.

Fig. 9 shows the absolute compressive strength versus the absolute density for the foam generated by the CFP method and steel foams produced by different techniques. When comparing steel foams produced by hollow spheres [9] with the CFP's foams, it can be seen (Fig. 9) that a 30% increase in the absolute density results in an increase of 260% in the absolute compressive strength. Given that scaling relations predict that the compressive strength of a closed cell foam should be directly proportional to its density [4], we may infer that the CFP foams have superior properties. Clearly, this result may be due to the fact that the cell wall material of the CFP foams is stronger; this point will be addressed in the following.

By normalizing the data, it is also possible to compare these results with values obtained from foams produced by other methods. This was achieved by dividing the foam density by the density of the cell wall material, and dividing the plateau stress (σ_p^*), by the compressive strength of the cell wall material. The density of the cell walls was taken as the density of iron (7.85 g/cm^3). The compressive strength of the ferrite cell wall material was estimated from hardness measurements. This was judged to be more accurate than taking a value from the literature, because of the possible presence of solid solution elements. Microhardness tests (100 g load) were carried out on the iron matrix of the cell walls using a Vickers indenter (LECO M-400 Hardness Tester);

TABLE II Comparison of relative compressive strengths and relative densities of iron foams prepared from CFP's, and steel foams generated using hollow spheres [8, 9] and the powder metallurgical method [7]. Notice that for comparison purposes the plateau stress (σ_p^*) was used instead of (σ_c^*).

Method	σ_p^*/σ_{CS}	ρ^*/ρ_s
Present study	0.10	0.23
Hollow spheres [8]	0.02	0.16
Hollow spheres [9]	0.05	0.21
P/M [7]	0.28	0.43

the duration of loading was 15 s. The average Vickers (VHN) and Brinell hardness numbers (BHN) were 214 ± 15 and 212 ± 12, respectively. Given that for steels, the tensile strength (when expressed in kg/mm^2) is approximately one third the BHN [21], this corresponds to an estimated tensile strength of 692 MPa for the foam cell wall material. For both iron and 1020 steel, the ratios of the yield strength to the tensile strengths are very similar, i.e. 0.48 [22]. Assuming this value is also applicable for the foam cell wall material gives a compressive yield strength value of 332 MPa. This value is 30% higher than accepted values for the yield strength of ferrite (252 MPa [23]). In terms of a direct comparison of the hardness values, the hardness measured experimentally on the foam cell walls was 15% higher than quoted values for the HB hardness of ferrite (184 HB [23]). These observations are consistent with a degree of solid solution hardening in the CFP foams. The normalized compressive strength value (σ_p^*/σ_{CS}) is thus 0.10.

Table II shows comparative results of relative compressive strength (σ_p^*/σ_{CS}) values, and corresponding relative densities (ρ^*/ρ_s), for steel foams produced by different methods. The relatively high value of (σ_p^*/σ_{CS}) for the P/M foam is not unexpected, since its relative density is twice the relative density of the foam produced by the CFP process. Therefore, σ_p^* is 69.21 MPa for the P/M foams, a value which is approximately twice the compressive strength of the CFP foams (34 MPa). On the other hand, it can be seen that the properties of foams produced from CFPs compare favorably with those derived from hollow spheres. Because the strength values have been normalized with respect to the cell wall material, it is reasonable to infer that any enhancement in behavior can be attributed to the cell morphology. Indeed, one of the proposed advantages of the CFP process is that there may be less 'waviness' in the cell walls compared to foams produced by the foaming of metals in the molten state. Other advantages of the process are the uniform cell morphology, and the relatively low value of the relative densities which can be achieved, particularly in comparison to steel foams produced by the powder metallurgy process [7]. Work is currently ongoing to achieve even lower densities by exploring faster setting cement formulations.

5. Summary

A novel approach has been developed to fabricate metal foams beginning with a ceramic foam precursor consisting predominantly of iron (III) oxide. This precursor was reduced at 1240°C in a 4% H_2-argon mixture to generate a closed cell iron foam with a uniform morphology. The relative density of the foam was 0.23 ± 0.017, and the average cell size was 1320 ± 320 mm. The hardness of the cell walls was determined by microhardness testing, and found to be ~214 VHN (212 BHN). The compressive stress-strain behavior of the iron foams was typical of cellular materials; the average compressive strength obtained was 29 ± 7 MPa.

Acknowledgments

The financial support of the U.S. Office of Naval Research (contract #N00014-01-1-0956, monitored by Dr. R. Barsoum) and the PA Department of Community and Economic Development is gratefully acknowledged. The authors are grateful to Arlan Benscoter for his assistance with the metallographic examination of the foams.

References

1. J. BANHART, *Prog. Mat. Sci.* **46** (2001) 559.
2. J. BANHART and D. WEAIRE, *Phys. Today*. **55** (2002) 37.
3. H. P. DEGISCHER and B. KRISTZ, in "Handbook of Cellular Metals: Production, Processing, Applications" (Wiley, New York, 2002) p. 1.
4. L. J. GIBSON and M. F. ASHBY, in "Cellular Solids" (Cambridge University Press, New York, 1997) p. 175.
5. M. F. ASHBY, A. EVANS, N. A. FLECK, L. J. GIBSON, J. W. HUTCHINSON and H. N. G. WADLEY, in "Metal Foams: A Design Guide" (Butterworth-Heinemann, Boston, 2000) p. 61.
6. T. MIYOSHI, M. ITOH, S. AKIYAMA and A. KITAHARA, in Materials Research Society Symposium Proceedings, San Francisco, April 1998, edited by D. S. Schwartz, D. S. Shih, A. G. Evans, and H. N. G. Wadley (MRS, Warrendale, 1998), p. 133.
7. C. PARK and S. R. NUTT, *Mat. Sci. Eng.* **A288** (2000) 111.
8. K. M. HURYSZ, J. L. CLARK, A. R. NAGEL, C. U. HARDWICKE, K. J. LEE, J. K. COCHRAN and T. H. SANDERS, in Materials Research Society Symposium Proceedings, San Francisco, April 1998, edited by D. S. Schwartz, D. S. Shih, A. G. Evans, and H. N. G. Wadley (MRS, Warrendale, 1998), p. 191.
9. O. ANDERSEN, U. WAAG, L. SCHNEIDER, G. STEPHANI and B. KIEBACK, *Adv. Eng. Mat.* **2** (2000) 192.
10. T.-J. LIM, B. SMITH and D. L. MCDOWELL, *Acta Mater.* **50** (2002) 2867.
11. A. VERDOOREN, H. M. CHAN, J. L. GRENESTEDT, M. P. HARMER and H. S. CARAM, in Cellular Metals: Manufacture, Properties, Applications/Proceedings of the International Conference on Cellular Metals and Metal Foaming, Berlin, June 2003, edited by J. Banhart, N. Fleck, and A. Mortensen (Verlag MIT Publishing, Berlin, 2003) p. 243.
12. H. MOTOKI, US Patent 4,084,980 (1978).
13. T. FINCH and J. H. SHARP, *J. Mat. Sci.* **24** (1989) 4379.
14. K. A. SHEHATA and S. Y EZZ, *Trans. Inst. Min. Met.* **82** (1973) C-38.
15. A. A. EL-GEASSY, K. A. SHEHATA and S. Y. EZZ, *Trans. ISIJ*. **17** (1977) 629.
16. N. G. GALLEGOS and M. A. APECETCHE, *J. Mat. Sci.* **23** (1988) 451.
17. H.-Y. LIN, Y.-W. CHEN and C. LI, *Therm. Acta*. **400** (2003) 61.

18. R. L. STEPHENSON and R. M. SMAILER, in "Direct Reduced Iron: Technology and Economics of Production and Use" (Iron & Steel Society of AIME, Warrendale, 1980) p. 25.
19. E. E UNDERWOOD, in "Quantitative Stereology" (Addison-Wesley, Reading, 1970) p. 90.
20. A. RAVAGLIOLI and A. KRAJEWSKI, in "Bioceramics: Materials, Properties, Applications" (Chapman and Hall, London, 1992) p. 57.
21. D. TABOR, in "The Hardness of Metals" (Oxford, London, 1951) p. 17.
22. W. D. CALLISTER JR., in "Materials Science and Engineering an Introduction" (Wiley, New York, 2003) p. 129.
23. ASM International Handbook Committee, in "Metals Handbook, Properties and Selection: Irons, Steels, and High Performance Alloys, Volume 1" (ASM International, Materials Park, 1990) p. 36.

Received 7 April 2004
and accepted 24 March 2005